Occludin Independently Regulates Permeability under Hydrostatic Pressure and Cell Division in Retinal Pigment Epithelial Cells

Brett E. Phillips,[1] Limary Cancel,[2] John M. Tarbell,[2] and David A. Antonetti[1,3]

PURPOSE. The aim of this study was to determine the function of the tight junction protein occludin in the control of permeability, under diffusive and hydrostatic pressures, and its contribution to the control of cell division in retinal pigment epithelium.

METHODS. Occludin expression was inhibited in the human retinal pigment epithelial cell line ARPE-19 by siRNA. Depletion of occludin was confirmed by Western blot, confocal microscopy, and RT-PCR. Paracellular permeability of cell monolayers to fluorescently labeled 70 kDa dextran, 10 kDa dextran, and 467 Da tetramethylrhodamine (TAMRA) was examined under diffusive conditions or after the application of 10 cm H_2O transmural pressure. Cell division rates were determined by tritiated thymidine incorporation and Ki67 immunoreactivity. Cell cycle inhibitors were used to determine whether changes in cell division affected permeability.

RESULTS. Occludin depletion increased diffusive paracellular permeability to 467 Da TAMRA by 15%, and permeability under hydrostatic pressure was increased 50% compared with control. Conversely, depletion of occludin protein with siRNA did not alter diffusive permeability to 70 kDa and 10 kDa RITC-dextran, and permeability to 70 kDa dextran was twofold lower in occludin-depleted cells under hydrostatic pressure conditions. Occludin depletion also increased thymidine incorporation by 90% and Ki67-positive cells by 50%. Finally, cell cycle inhibitors did not alter the effect of occludin siRNA on paracellular permeability.

CONCLUSIONS. The data suggest that occludin regulates tight junction permeability in response to changes in hydrostatic pressure. Furthermore, these data suggest that occludin also contributes to the control of cell division, demonstrating a novel function for this tight junction protein. (*Invest Ophthalmol Vis Sci.* 2008;49:2568–2576) DOI:10.1167/iovs.07-1204

The blood-retinal barrier is composed of epithelial cells of the retinal pigment epithelium and endothelial cells of the retinal vasculature that are under transmural hydrostatic pressure gradients and are composed of cells with a very low mitotic index with well-developed tight junctions. Tight junctions establish physiological barriers that regulate the movement of ions, small solutes, and fluid between tissue compartments.[1,2] The retinal pigment epithelium contributes to the outer portion of the blood retinal barrier,[3,4] and the retinal pigment epithelial (RPE) dysfunction caused by tight junction opening and increased permeability results in macular edema associated with retinitis pigmentosa.[5–8]

Transmembrane proteins that contribute to tight junction barrier properties include claudins, tricellulin, and occludin.[9–12] Occludin is a tetraspan transmembrane protein located at tight junctions but its precise cellular functions remain unclear. Changes in occludin content correlate with altered permeability, making occludin a likely regulator of overall paracellular permeability of the tight junction.[13–16] Similarly, the loss of occludin protein is associated with a number of abnormalities such as diabetic retinopathy[14] and inflammatory bowel disease.[17] Treatment of RPE cells with hepatocyte growth factor[18] or interleukin-1β[19] reduced occludin content associated with increased permeability. Furthermore, treatment of ARPE19 cells with matrix metalloproteinases 2 and 9, two proteinases elevated in the retina in diabetes, specifically decreased occludin content and increased permeability.[20] These studies demonstrate that cytokines and proteinases that are altered in a number of retinal diseases, including diabetic retinopathy, reduce occludin content associated with increased permeability.

The contribution of occludin to barrier properties remains controversial. Blocking the extracellular loops[21–25] and reducing the protein content[26] of occludin alter paracellular permeability in a number of cell systems. Occludin-deficient mice are viable; tight junction ultrastructure appears unaltered, and isolated intestinal tissues demonstrate normal transepithelial resistance (TER) and permeability to mannitol. These mice do, however, display a number of aberrant phenotypes in tissues containing tight junctions, including testicular atrophy in males, inability to suckle in females, gastric mucus cell hyperplasia, and calcification of the brain.[27,28] Additional evidence for occludin in regulating epithelial cell division has been suggested by the ability of exogenous occludin expression to revert the phenotype of raf-transformed rat salivary gland epithelial cells.[29]

Most occludin permeability studies are performed at or near atmospheric pressure, and the role of occludin has yet to be assessed under a transmural pressure gradient that more closely models physiological conditions. The net movement of water across tissue barriers is governed by differential fluid and oncotic pressure, as expressed in Starling's equations and subsequent adaptations (for a review, see Salathe[30]). Application of a transmural hydrostatic pressure gradient across endothelial cell monolayers rapidly increases effective permeability of solutes through convective forces. However, during the 30 to 60 minutes after pressurization, the endothelial cells respond by reducing effective solute and water permeability.[31–33] This sealing effect[34] is an adaptive biological response to changes in

hydrostatic pressure.[33] In the present study, the contribution of occludin to regulation of the blood-retinal barrier after application of hydrostatic pressure was examined using the RPE cell line ARPE-19. This cell line has well-developed tight junctions in stable monolayers.[3,4] In addition, these studies addressed the novel hypothesis, suggested by occludin knockout mice, that occludin may contribute to growth control, and they examined the relationship of growth control to permeability under diffusive conditions.

MATERIALS AND METHODS

Cell Culture and Electroporation

ARPE-19 cells (ATCC, Manassas, VA) were grown in DMEM/F-12 Ham media with L-glutamine and 15 mM HEPES (Sigma, St. Louis, MO) and were supplemented with 1.16 g/L sodium bicarbonate, 10% FBS, and antibiotic-antimycotic (Gibco BRL, Rockville, MD). The introduction of siRNA was achieved using 5.0×10^5 cells in an electroporator (Nucleofector II, program number L-23 [Amaxa, Cologne, Germany] with Nucleofector Kit V). Each reaction received 10 pmol human silencer negative control siRNA 1 or occludin siRNA 143665 (Ambion, Austin, TX). Transfection efficiency was tested using plasmid for enhanced green fluorescence protein and a fluorescence-labeled small RNA oligonucleotide; in both cases, it was near 100% with repeat experiments. Unless stated otherwise, cells were plated on six-well Costar (Cambridge, MA) tissue culture plates at a density of 5.0×10^5 cells/well and were harvested 4 days after electroporation. Confluence of the ARPE-19 cell monolayer was confirmed by observation with a phase-contrast microscope 1 day after plating. Three days after plating, cells were washed twice with phosphate-buffered saline (PBS) and were fed with serum-free media. All cell assays were on day 4 after electroporation. To inhibit the cell cycle, cells were treated with DMSO containing 5 μM aphidicolin (Calbiochem, San Diego, CA), or 10 μM roscovitine (Calbiochem) for 4 hours.

Protein Quantification

Relative protein content was quantified by Western immunoblotting. Cells were harvested in a detergent-based extraction buffer, and total protein concentrations were determined as previously described.[35] The Western gel system (NuPAGE; Invitrogen, Carlsbad, CA) was used to separate proteins. Forty micrograms protein was diluted in LDS sample buffer (NuPAGE, Invitrogen) and was loaded on 4% to 12% Bis-Tris 1.5-mm, 10-well gels (NuPAGE, Invitrogen). The gels were run according to NuPAGE protocols using MOPS SDS running buffer (Invitrogen). The gels were then transferred to MSI nitrocellulose (Fisher Scientific, Pittsburgh, PA), blocked in 5% fat-free milk in TBST, and immunoblotted with polyclonal rabbit ZO-1 (N-term; 1:150), polyclonal rabbit Claudin-1 (1:150; Invitrogen), or monoclonal mouse occludin (1:1000; BD Biosciences, San Jose, CA). Primary antibodies were detected with alkaline phosphatase-conjugated anti-mouse IgG and chemifluorescence or horseradish peroxidase-conjugated anti-rabbit IgG and chemiluminescence (ECL Plus; GE Healthcare, Buckinghamshire, England). Results were analyzed using acquisition software (ImageQuant 5.2 [Molecular Dynamics, Sunnyvale, CA] or Genesnap [SynGene, Frederick, MD]) software.

RNA and DNA Quantification

RNA was quantified using real-time PCR. RNA was collected using an RNA isolation kit (ToTALLY RNA Kit; Ambion, Austin, TX). RNA integrity and concentration were determined using a bioanalyzer (Agilent 2100; Agilent Technologies, Santa Clara, CA). cDNA was made from 1 μg total RNA with oligo-DT primers using a system for the synthesis of high-quality first-strand cDNA (Super Script III First-Strand Synthesis Systems for RT-PCR; Invitrogen). To quantify mRNA content, reactions containing 200 ng cDNA in a total volume of 10 μL were assessed with gene expression assay (TaqMan; Applied Biosystems, Foster City, CA) in combination with a PCR system (7900HT Fast Real-Time PCR System; Applied Biosystems). Gene expression primer sets used were as follows: occludin Hs00170162_m1, claudin-1 Hs00221623_m1, claudin-2 Hs00252666_s1, ZO-1 Hs00268480_m1, E-cadherin Hs00170423_m1, and cyclophilin A Hs99999904_m1 (Applied Biosystems). Cyclophilin A was used as an endogenous housekeeping gene for normalization between samples. Relative mRNA content was determined using the $\Delta\Delta C_t$ method in the SDS 2.2 software (Applied Biosystems).[36]

DNA content was measured using an assay kit protocol (Quant-iT Pico Green dsDNA Assay; Invitrogen). Cells were plated on 13-mm diameter, 24-well tissue culture plates at a density of 1.0×10^5 cells/well. On day 4, media were collected, and cell lysates were collected as described. Standard curves incorporated either media or lysis buffer as appropriate.

Immunocytochemistry

Cells were plated on 12-mm diameter glass coverslips (Fisher Scientific) at a density of 1.5×10^5 cells/well. At day 4 after electroporation, cells were fixed in 1% paraformaldehyde for 10 minutes as previously described.[35] Coverslips were incubated in PBS, 10% goat serum, and 0.1% Triton X-100 with rat anti-ZO-1 mAb culture supernatant (1:4), rabbit anti-Ki67 (1:1000; Visionbiosystems, Norwell, MA), and monoclonal mouse occludin IgG (1:200; Invitrogen) for 3 days. Detection of primary antibodies was with Alexa 488 anti-mouse, Alexa 555 anti-rabbit, and Alexa 647 anti-rat antibodies (Invitrogen), and DNA was detected with Hoechst stain (1:1000) for 1 hour. Cells were imaged on a confocal microscope (TCS SP2 AOBS; Leica; Wetzlar, Germany). Cell density was calculated by dividing the total cell number by the field surface area (0.1406 mm^2). The percentage of Ki67-positive cells was calculated by dividing Ki67-positive cells by total Hoechst-stained cells in a given field. Nine total fields were counted per condition across three coverslips.

Diffusive RPE Permeability and TER Measurements

Cells were plated on 12-mm diameter, 0.4-μm pore size, polyester transwell filters (Costar) at 1.0×10^5 cells/well. TERs were measured using an EVOM with a STX2 Electrode (World Precision Instruments, Sarasota, FL) on day 4 before solute permeability experiments. Dextran diffusive permeability rates were determined by placing 10 μM of 70 kDa (Sigma) or 10 kDa (Invitrogen) RITC-dextran in the apical transwell chamber. Every 30 minutes, 50-μL aliquots were collected from the basolateral chamber for 3.5 hours. At the final time point, a 50-μL aliquot was collected from the apical chamber. Fluorescence aliquots were quantified (FluorImager 595; Molecular Dynamics), and diffusive permeability rates (P$_o$) in centimeters per second were calculated as previously described.[35]

Measurement of 467-Da TAMRA permeability required quantification of the changing apical TAMRA concentration over the course of the experiment. Aliquots were collected every 15 minutes from the basolateral chamber and every 30 minutes from the apical chamber for 2 hours. Apical chamber concentrations were fit to a linear regression, and the time-averaged apical fluorescence across each 15-minute interval was used to calculate the P$_o$ as follows:

$$P_o = [(\Delta F_A/\Delta t)V_A]/(F_{Lt}A) \qquad (1)$$

where P$_o$ is diffusive permeability (cm/s), ΔF_A is the change in basolateral fluorescence, F_{Lt} is apical fluorescence at 15-minute intervals, Δt is the change in time (15-minute intervals), V_A is basolateral chamber volume (cm^3), and A is filter surface area (cm^2).

RPE Permeability Measurements under Transmural Pressure

Measurement of 70-kDa RITC dextran and 467-Da TAMRA permeability across RPE cell monolayers under 10 cm H$_2$O pressure was achieved

using a sealed chamber coupled to a fiber-optic light detection system, as previously described with subsequent modifications.[33] Briefly, a fiber-optic lead directs 532-nm light provided by a 10 mW crystal laser to the basolateral chamber below the transwell filter. A second fiber-optic lead carries light from the basolateral chamber to a photon-counting detector (C&L Instruments, Hummelstown, PA) after passage through a 571-nm high-pass filter for real-time measurement of fluorescent solute permeability across the cell monolayer. The basolateral chamber connects to hydraulic tubing, allowing for a pressure differential to be applied across the cell monolayer. The system accommodates eight chambers to simultaneously measure solute permeability. Cell monolayers were placed in the chambers for 1 hour without pressure for equilibration before the application of pressure, serum-free media were used as described with the addition of 1% BSA, and 10 cm H_2O pressure was applied for 2 hours. For permeability measurements, the apical media chamber received 1.44 μM of 70-kDa RITC-dextran or 480 nM TAMRA. Initial fluorophore concentrations were selected to produce fluorescence readings within the photon-counting detector range. RITC-dextran (70 kDa) was added to the apical chamber at the beginning of equilibration before pressure application. TAMRA was added to the apical chamber 1 hour after pressure application because the apical TAMRA concentration was depleted too quickly to apply TAMRA earlier. Fluorescence intensity measurements for the basolateral chamber were smoothed using the *supsmooth* function from Mathcad 13 (Cambridge, MA), converted to nM concentrations based on standard curves generated for each cell chamber, and averaged into 5-minute intervals. Effective permeability rates (P_e) were calculated in cm/s units, as previously described.[37] Statistical analysis (Prism 4.02 software; GraphPad Software, San Diego, CA) was conducted using both ANOVA and area under the curve (AUC) analyses with baseline set at 0 and two-tailed *t*-test.

Cell Viability and DNA Synthesis Measurements

To measure DNA synthesis, cells were plated on 13-mm diameter, 24-well tissue culture plates at a density of 1.0×10^5 cells/well. On day 4 after electroporation, monolayers with 2 μCi tritiated thymidine added to 500 μL media in each well were incubated for 2 hours at 37°C. The cells were then washed with PBS, and the nucleic acid was precipitated with 300 μL of 10% trichloric acid (TCA) for 10 minutes at 25°C. The TCA was aspirated, and the precipitates were solubilized in 0.2 M NaOH with 40 μg/mL DNA type I for 30 minutes at 37°C. The solution was transferred to a scintillation counter, and disintegrations per minute was read for 1 minute (LS 6000SC; Beckman Coulter, Fullerton, CA). Relative thymidine incorporation after background subtraction was analyzed by *t*-test. Cells were assayed (Live/Dead Viability/Cytotoxicity Kit for Animal Cells; Invitrogen) according to the supplied protocol. For positive control of cell death, cells were treated with 70% ethanol for 30 minutes.

Cell viability was also assessed using fluorescence-activated cell sorting. Cells were lightly trypsinized in a 0.5× trypsin solution until the cells lifted off the plate. A detection kit (Annexin V-PE Apoptosis Detection Kit I; BD Biosciences) was used to label the cells according to the manufacturer's protocol and were read on a FACScan (BD Biosciences). Standard quadrant analysis was performed, and all cells stained for Annexin V-PE and 7-AAD were pooled to represent the number of dead cells.

Electron Microscopy

Cells were plated on 24-mm diameter, 0.4-μm pore size, polyester transwell filters (Costar) at 5.0×10^5 cells/well. Cells were pressurized to 10 cm H_2O for 2 hours before fixation. The apical media chamber contained 2 mL media. To the apical chamber, 4 mL of 4% paraformaldehyde, 1% glutaraldehyde (Electron Microscopy Science, Hatfield, PA), and 0.1 M sodium cacodylate buffer (Fisher Scientific) was added. Cells were fixed in this solution for 1 hour under pressure along with nonpressurized transwell filters in six-well tissue culture plates. After 1 hour of fixation, the pressure was removed, and all filters were washed

in 0.1 M sodium cacodylate. Undiluted fixative was then applied to all filters for an additional 20 minutes. Cells were washed with 0.1 M sodium cacodylate and postfixed with a 1% osmium and 1.5% potassium ferrocyanide solution in 0.1 M sodium cacodylate overnight. The cells were then dehydrated with progressively increasing concentrations of ethanol and imbedded in resin (Epon 812; Electron Microscopy Science). Sections were viewed and imaged under an electron microscope (model 400; Philips, Eindhoven, Netherlands). The presence or absence of pressure did not affect tight junction appearance in images (data not shown); therefore, only pressurized images are presented.

Statistical Analysis

Unless otherwise noted, statistical analysis was performed as follows. Within a data set, samples greater than 2 SD were discarded. A two-tailed *t*-test (two conditions) or ANOVA (three or more conditions) was performed using software for statistical analysis (InStat 3.05; Graph-Pad). $P < 0.05$, $P < 0.01$, and $P < 0.001$ were considered significant, as indicated in the figures and legends.

RESULTS

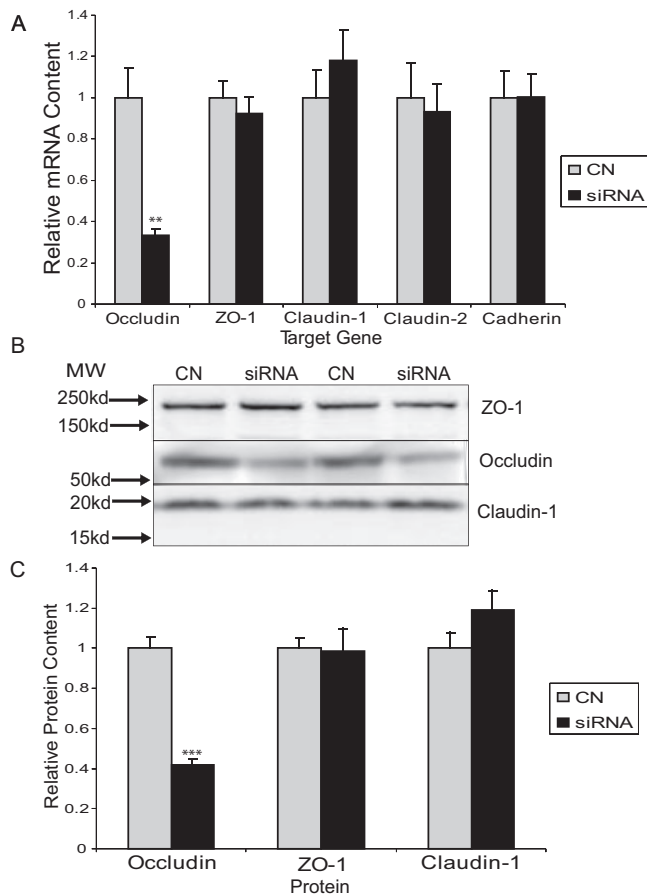### Tight Junction Protein Content after Occludin Depletion

ARPE-19 cells were transfected with occludin-targeted siRNA or a human negative control siRNA that did not match any sequence in the human genome. Four days after siRNA transfection, mRNA and protein content were examined. Occludin-targeted siRNA reduced occludin mRNA by 65% compared with control siRNA with no significant changes in mRNA of tight and adherens junction proteins ZO-1, claudin-1, claudin-2, or E-cadherin (Fig. 1A). Protein levels were quantified by Western blot analysis. Occludin protein content similarly decreased by 60% with occludin-targeted siRNA treatment with no change in ZO-1 or claudin-1 protein content (Fig. 1B). In preliminary experiments, ARPE-19 cells were compared with mock-transfected cells, scrambled siRNA for occludin, and occludin siRNA conditions. In these experiments, occludin reduction of 50% to 60% was observed in the occludin siRNA alone, not in any other conditions. Immunocytochemistry revealed that localization of ZO-1 at the plasma membrane did not change with reduced occludin content (Fig. 2A). Transmission electron micrographs of osmium tetroxide-stained ARPE19 cells, ARPE19 cells with control scramble RNA, or ARPE19 cells with occludin siRNA demonstrated tight junctions that appeared morphologically identical at the ultrastructural level (Fig. 2B). These data demonstrate the specificity of the siRNA and are consistent with the formation of tight junctions in occludin-deficient mice[27,28] and tissue culture studies.[26]

Permeability under Hydrostatic Pressure after Occludin Depletion

The effect of occludin depletion on permeability was tested under an atmospheric and a physiological transmural pressure gradient. Diffusive permeability of ARPE-19 cell monolayers was tested with a range of solute sizes after transfection with siRNA to occludin. Under diffusive conditions, occludin siRNA did not affect permeability to 70 kDa or 10 kDa RITC-dextran, whereas permeability to 467 Da TAMRA increased 15% (Fig. 3A). Cell monolayer TER was tested and declined 20% with occludin protein reduction (Fig. 3B). Thus, in the absence of a pressure gradient, the reduction of occludin content only increased diffusive permeability to 467 Da TAMRA.

Although the role of occludin in permeability has been previously examined under diffusive conditions, the contribution of occludin to the cell's response to a pressure differential

FIGURE 1. Junctional protein and mRNA content after occludin depletion. ARPE-19 cells were transfected with negative control (CN) or occludin-targeted siRNA (siRNA). Cells were harvested 4 days later, and mRNA and protein content were analyzed. (**A**) RT-PCR quantification, mean, and SE of the mean (SEM) of CN and siRNA-treated cells ($n = 6$). (**B**) Western blot analysis of ZO-1, occludin, and claudin-1. (**C**) Densitometric quantification of Western blot, mean, and SEM ($n = 3$). Of the junctional components examined, only the tight junctional protein occludin showed significant changes in mRNA and protein content. Two-tailed *t*-test was performed to determine significance. **$P < 0.01$; ***$P < 0.001$.

has yet to be examined. Although the pressure differential across the RPE is unknown, normal intraocular pressure ranges from 10 to 20 mm Hg. Permeability of ARPE-19 monolayers was tested under 10 cm H_2O pressure (7.35 mm Hg) after siRNA transfection. Previous studies have demonstrated fluid flow across the RPE from the retina to the choroid,[38,39] which is well vascularized and has vessels with low barrier properties. Therefore, the pressure used was slightly less than a normal pressure differential across the RPE assuming a negligible negative pressure from the choroidal side. Pressure application to cell monolayers initially results in a fourfold to sevenfold elevation of permeability to 70 kDa RITC-dextran, but the cells responded to the elevated pressure and reduced permeability over the next 60 minutes (Fig. 4A). This is the first demonstration that RPE cells, like endothelial cells,[33] display an adaptive response or a sealing effect to transmural pressure. Permeability after 60 minutes was analyzed statistically with ANOVA and AUC analysis. ARPE-19 cells under pressure with reduced occludin content demonstrated a 50% decrease in permeability to 70 kDa RITC-dextran compared with control siRNA-treated cells (Fig. 4A). Because preliminary experiments demonstrated TAMRA permeability was much higher than 70 kDa RITC

dextran, it was not possible to measure permeability over the same time course as for the larger molecule. Therefore, permeability was measured starting 60 minutes after pressure application because the cells appeared to reach equilibrium at this time point. In contrast to the larger molecule, TAMRA permeability increased 50% in occludin siRNA-treated cells compared with control cells (Fig. 4B).

The use of occludin siRNA altered the cell's response to the application of a transmural pressure gradient. Figure 4C shows a comparison of TAMRA and 70 kDa RITC-dextran permeability before and after pressure application. Normally, the cells responded to the elevated pressure and increased permeability with an adaptive response, reducing the permeability across the RPE monolayer for both small and large molecules. This adaptive response led to a final rate of permeability under transmural pressure nearly equal to the nonpressure conditions for the small molecule TAMRA, as seen in Figure 4C. However, with occludin siRNA, the permeability to 467 Da TAMRA was elevated 50% after the application of pressure, suggesting a reduced adaptive response. Meanwhile, an adaptive response was observed in the permeability to 70 kDa RITC-dextran after pressure application in control and siRNA-treated cells (Figs. 4A, 4C). After pressure, there was twofold greater permeability to 70 kDa RITC-dextran in control cells than in siRNA-treated cells. These data demonstrate that the retinal pigment epithelium differentially regulates permeability to 70 kDa dextran and the smaller 467 Da TAMRA molecules and that occludin has specific control of small molecule permeability.

Occludin siRNA Increases the Rate of Cell Division

Changes in cell division or cell number could potentially account for molecule-specific changes in permeability. Therefore, cell number, cell death, and rate of cell division were assessed in control and occludin siRNA-treated cells. Immunocytochemistry was performed with the Ki67 antibody to mark entry into the cell cycle (Fig. 5A). Cells were counterstained with Hoechst nuclear stain, and a ratio of Ki67 to Hoechst-stained cells was determined. Occludin siRNA significantly increased the number of Ki67-positive cells from 15% to 23% of the total (Fig. 5C), suggesting occludin reduction increases the number of cells undergoing active cell cycle. Reducing occludin content 65% with occludin siRNA also increased tritiated thymidine incorporation by 90% compared with controls (Fig. 5D), demonstrating increased DNA synthesis. This effect was dependent on the content of occludin because a separate siRNA to occludin (occludin siRNA 143664; Ambion) that reduced occludin content 38% increased tritiated thymidine incorporation 25% (data not shown). Together these data demonstrate that occludin contributes to the control of cell cycle in ARPE-19 cells.

Alterations in cell viability and cell death were examined to account for the change in cell cycle entry. Cell viability after occludin siRNA treatment was determined by flow cytometry in ARPE-19 cells. No significant difference existed in total number of viable or dead cells between control and occludin siRNA treatments (Fig. 5E). In addition, ARPE-19 monolayers were assessed for viability with calcein AM and cytotoxicity with ethidium bromide staining. No significant differences in monolayer cell viability or cell death were detected between control and occludin siRNA-treated cells (Figs. 5F, 5G), suggesting that cell viability was not compromised by the siRNA. The DNA content of ARPE-19 monolayers was unchanged (Fig. 5H), but culture media DNA content was twofold greater in occludin siRNA-treated cells (Fig. 5G), suggesting siRNA-treated monolayers maintain cell numbers by releasing excess cells into the media.

A

B
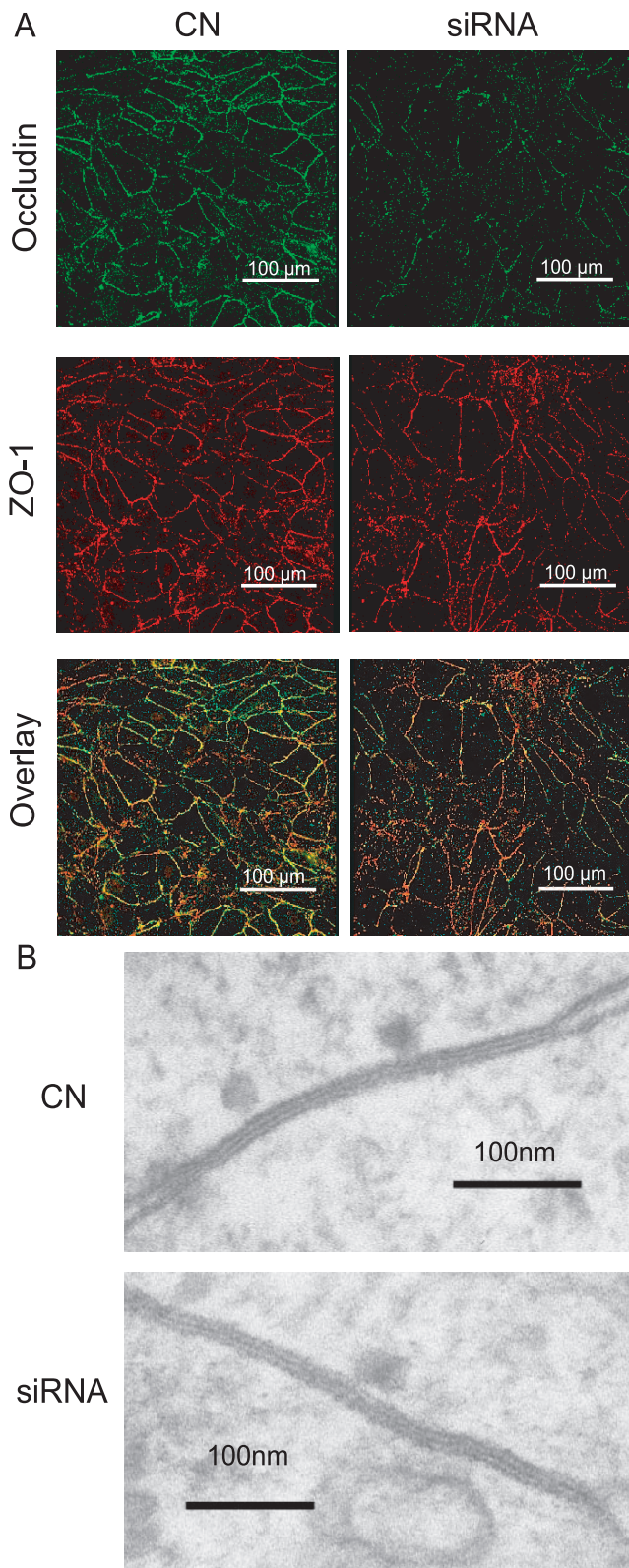
FIGURE 2. Occludin siRNA treatment did not inhibit ARPE-19 tight junction formation. ARPE-19 cells were treated with control negative and occludin-targeted siRNA (siRNA). Cells reached confluence 1 day after treatment and were fixed on day 4. (**A**) Immunocytochemistry was performed on ARPE-19 monolayers for tight junction proteins occludin (*green*) and ZO-1 (*red*). Occludin content and localization at the plasma membrane were reduced with occludin siRNA treatment, while ZO-1 was unaffected. (**B**) Sections were cut perpendicularly to

## Permeability Is Independent of the Rate of Cell Division

The increased rate of cell division in occludin siRNA-treated cells could contribute to ARPE-19 paracellular permeability; therefore, two cell cycle inhibitors were selected to block cell division. Aphidicolin is a DNA polymerase I inhibitor that stops cells in the early S phase of the cell cycle. Roscovitine is a cyclin-dependant kinase inhibitor that stops cells in the early S and mitotic phases of the cell cycle. Figure 6A shows the relative amount of tritiated thymidine incorporation after 4 hours of treatment with 5 μM aphidicolin, 10 μM roscovitine, or an equal volume of vehicle control DMSO. Occludin siRNA increased thymidine incorporation by 70%, similar to previous results (Figs. 5D, 6A). DNA synthesis was blocked by 90% with 5 μM aphidicolin and 70% with 10 μM roscovitine (Fig. 6A). The TER measured across the cell monolayer was unaffected by drug treatment, suggesting increased cell division did not account for the reduced TER after occludin siRNA treatment (Fig. 6B). Similarly, diffusive permeability to 70 kDa RITC-dextran was unaffected by reductions in cell division rates (Fig. 6C). The increase in diffusive TAMRA permeability after occludin siRNA treatment was not affected by aphidicolin (Fig. 6D) or roscovitine (Fig. 6E) treatment. These data suggest that the permeability changes resulted from reduced occludin content at the junction and not from increased proliferation.

DISCUSSION

The major findings of this study were that occludin regulates cell proliferation and paracellular permeability in ARPE-19 cells under physiological hydrostatic pressure. Numerous experimental models have examined the role of the tight junction protein occludin in regulating paracellular permeability, demonstrating a strong correlation between occludin content and permeability characteristics[13,14] and providing experimental evidence for occludin in contributing to barrier properties.[40,41] However, gene deletion experiments have found little evidence of occludin in establishing barrier properties.[27,28] Recent evidence has pointed to a role for occludin in regulating cell growth, including increased gastric mucus cell hyperplasia after occludin knockout[27,28] and reversion of the raf-transformed phenotype by exogenous expression of occludin.[29] Further, occludin directs TGFβR1 to the tight junction, which is required for TGFβ-induced epithelial-to-mesenchymal cell transition.[42] Here an siRNA to occludin was used in ARPE-19 cells to reduce occludin content by transient transfection to examine the contribution of occludin to blood-retinal barrier properties under conditions of a hydrostatic pressure gradient and to examine the contribution of occludin depletion to growth control. We report that occludin contributes to the regulation of barrier properties under hydrostatic pressure and also to the regulation of cell division.

The reduction in occludin protein content increased permeability to the small 467 Da TAMRA molecules but had no effect on permeability to RITC-dextran molecules of 70 kDa and 10 kDa under diffusive conditions. This is similar to findings in MDCK II cells with constitutive ablation of occludin protein.[26] The application of occludin-blocking peptides in various tissue culture models has also demonstrated increases in small molecule permeability[23,24] and in larger 3-kDa and

the plane of the fixed cell monolayer and were examined by electron microscopy. These images were of cells exposed to transmural 10 cm H$_2$O pressure before fixation. Nonpressurized cells were similar in appearance (data not shown).
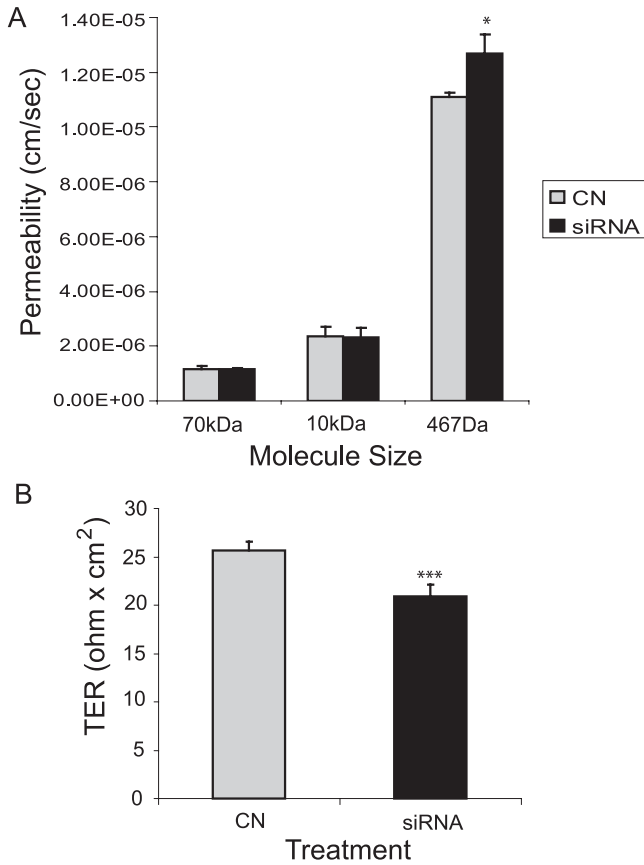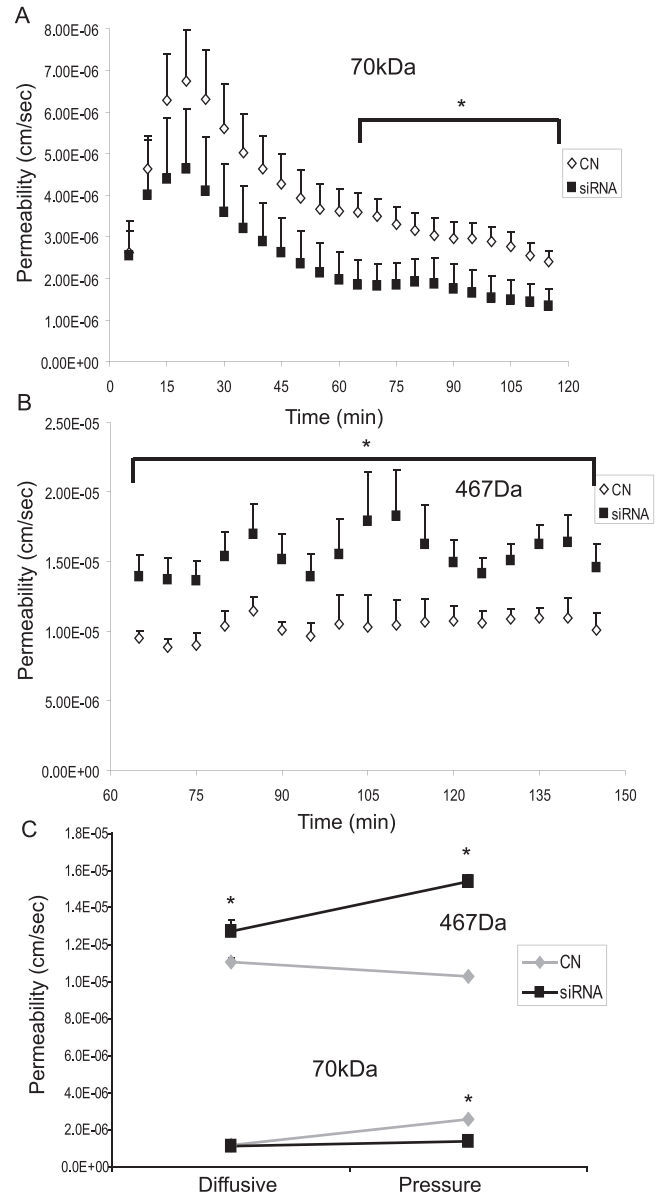
FIGURE 3. Diffusive paracellular permeability of ARPE-19 monolayers is modestly affected by occludin siRNA treatment. Graphs display permeability mean and SEM. (**A**) Paracellular permeability to 70 kDa ($n = 20$) and 10 kDa ($n = 10$) RITC-dextran molecules was measured over a 3.5-hour time course and the 467 Da TAMRA ($n = 15$) over a 2-hour time course. (**B**) ARPE-19 monolayer TER was measured twice per transwell filter and averaged ($n = 32$). Two-tailed *t*-test was performed to determine significance. $*P < 0.05$; $***P < 0.001$.

40-kDa dextran molecules in some studies.[21,23] Surprisingly, occludin-deficient mice do not display increased permeability to mannitol in isolated intestinal epithelia despite a number of phenotypic defects associated with tissues containing tight junctions.[27,28] The difference in this study and the knockout mice may be attributed to cell context, as was demonstrated with claudin gene depletion,[43] or perhaps from a difference in transient depletion compared with development with occludin gene deletion. The present results examining permeability under diffusive conditions agree with many of the previous studies demonstrating that blockade of occludin increases small molecule and ion permeability with a modest 15% to 20% change.

The effect of occludin depletion on tight junction permeability has not been previously tested under physiological pressure. The hydrostatic pressure present in physiological microenvironments of cell and tissue barriers affects the net movement of water and solutes across tissues. Previous studies have demonstrated that the application of pressure results in increased ZO-1 immunoreactivity at the cell border and a subsequent sealing to water and solute permeability in endothelial cells.[33] The results of the present study are the first demonstration of this adaptive sealing response in epithelial cells. However, though control RPE cells also resisted an increase in permeability of TAMRA after the application of transmural pressure, the occludin-depleted cells demonstrated an

increase in permeability to TAMRA after pressure. These data suggest that occludin is necessary for the cell's adaptive response to changes in pressure. Interestingly, occludin deple-

FIGURE 4. Occludin dynamically regulates paracellular permeability under hydrostatic pressure. (**A**). Ten centimers H$_2$O transmural pressure was applied to ARPE-19 monolayers at 0 minutes, and permeability to 70 kDa was calculated over 5-minute time intervals for 2 hours (CN, $n = 8$; siRNA, $n = 7$). Pressure application initially resulted in a fourfold to sevenfold elevation of permeability to 70 kDa dextran, followed by a reduction over the next 60 minutes. Statistical significance was determined from 65 to 115 minutes by two-way ANOVA ($P < 0.05$) and two-tailed *t*-test performed on AUC values ($P < 0.01$). (**B**) ARPE-19 permeability to 467 Da TAMRA was measured starting 1 hour after pressure application, and statistical significance was determined over 65 to 145 minutes (ANOVA, $P < 0.05$; AUC, $P < 0.05$; CN, $n = 6$; siRNA, $n = 8$). (**C**) Comparison of diffusive permeability (Fig. 3A) and average permeability under pressure (over the same timeframe described) for 70 kDa dextran and TAMRA permeability. Statistical significance was determined as stated ($*P < 0.05$). Occludin siRNA treatment increased permeability to TAMRA in diffusive and pressured conditions but decreased permeability to 70kDa RITC-dextran compared with control-treated cells under pressure, suggesting occludin dynamically regulates permeability.
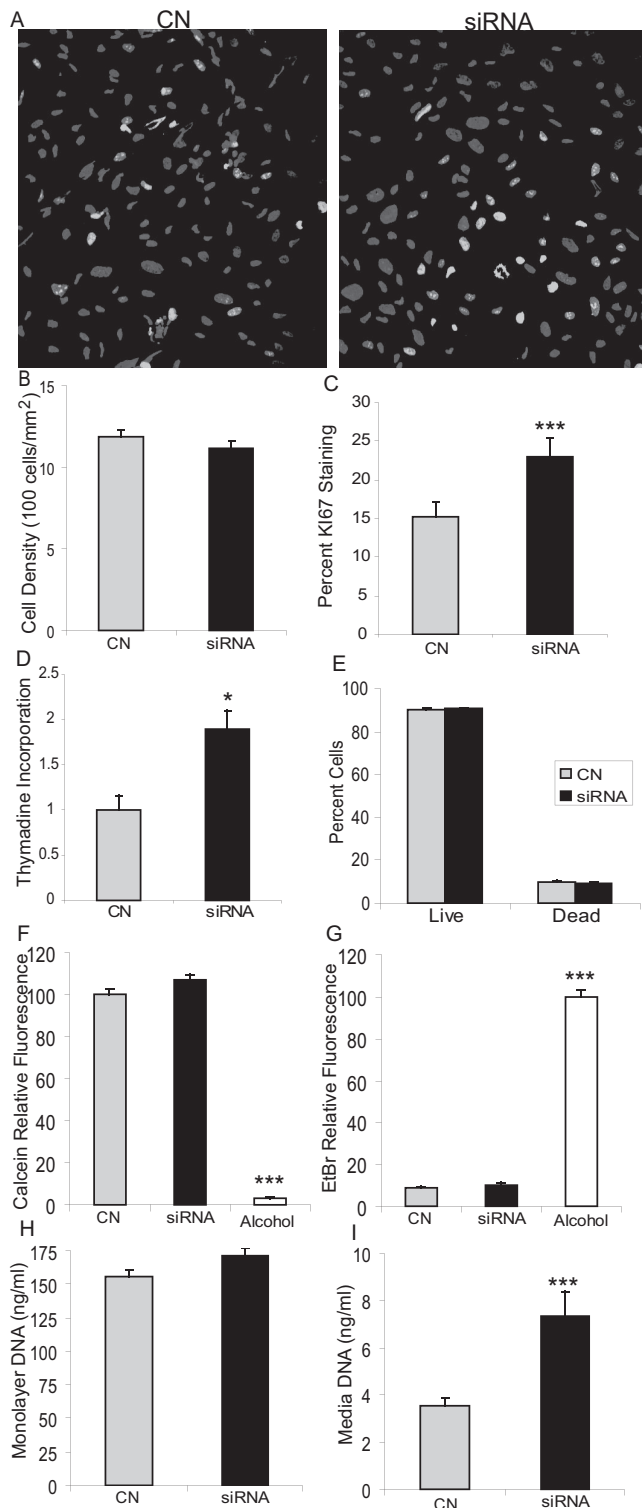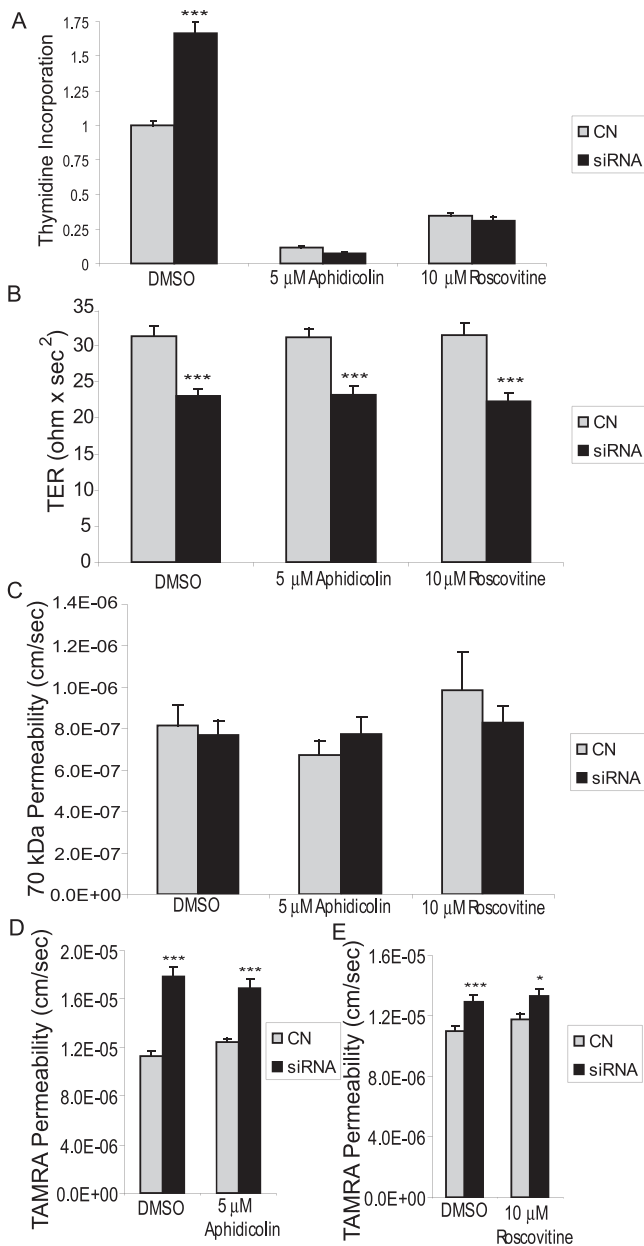
FIGURE 5. ARPE-19 cell division rates increase after occludin siRNA treatment. ARPE-19 cells were treated with control (CN) and occludin-targeted siRNA (siRNA). Graphs display mean and SEM values. (**A**) Immunocytochemistry was performed with Hoechst nuclear stain (*gray cells*) and Ki67 antibody (*white cells*) on confluent ARPE-19 monolayers. Ki67 is a nuclear protein expressed only in actively dividing cells during the G1, S, G2, and mitotic cell cycle phases. (**B**) Cell density was quantified by counting the number of Hoechst-stained cells per field and was unchanged between treatment conditions ($n = 3$). (**C**) The percentage of cells that stained positive for Ki67 increased 50% with occludin siRNA treatment compared with the control scrambled treatment ($n = 3$). (**D**) ^{3}H-thymidine incorporation over 2 hours

increased 90% in occludin siRNA-treated cells compared with control scrambled-treated cells ($n = 12$). (**E**) Flow cytometry was performed on resuspended ARPE-19 monolayers (CN, $n = 7$; siRNA, $n = 8$). Cells were labeled with Annexin V-PE, which binds to the phosphatidylserine exposed on the cell membrane surface during early apoptosis, and the vital cell dye 7-AAD, which is excluded from living cells. Quadrant analysis was performed, and cells stained positively for Annexin V or 7-AAD were designated as dead, whereas unstained cells were designated as live. ARPE-19 monolayers were incubated with (**F**) calcein, which is taken up by living cells, and (**G**) ethidium bromide, which is excluded from living cells (CN, $n = 9$; siRNA, $n = 8$; alcohol, $n = 4$). A positive cell death control was treated with 70% ethanol for 30 minutes. Relative incorporation was measured with a spectrophotometer. No significant difference in cell viability existed between siRNA-treated and control APRE-19 cells. DNA content was measured in APRE-19 (**H**) cell monolayers and (**I**) cell culture media on cells from day 3 to day 4 after siRNA treatments ($n = 6$). DNA content did not change in the cell monolayer but significantly increased twofold in cell media from control scrambled-treated to occludin siRNA-treated cells. These data demonstrate occludin siRNA treatment increased cell division rates without changing cell number or viability within ARPE-19 monolayers compared with control. Excess cells are released into the media. Two-tailed *t*-test or ANOVA (if more than two conditions) was performed to determine significance (*$P < 0.05$; ***$P < 0.001$).

tion in MDCK II cells altered the cell's response to cholesterol depletion.[26] Together, these studies suggest a role for occludin in signaling changes in barrier properties in response to external signals.

In contrast to TAMRA, permeability to 70 kDa dextran was reduced in occludin siRNA-treated cells after pressure application when compared with controls, though both conditions adapted to the elevated pressure. It is not clear what caused this unexpected decrease in 70 kDa dextran paracellular permeability in occludin-siRNA treated cells, but one possibility is that there were compensatory changes in the adherens junction after occludin depletion. Adherens junctions restrict large molecule permeability in the absence of a functional tight junction,[44,45] but it is not clear why the reduction of occludin would result in the strengthening of the adherens junction. One possibility is that ZO-1 moves from the tight junction to the basal adherens junction with the loss of occludin. The same SH3-linked guanylate kinase domain of ZO-1 binds either occludin or the adherens junction protein α-catenin.[46] Increased transcription of the adherens junction protein β-catenin has also been observed after the loss of occludin at the plasma membrane.[22] The results reported here suggest that TAMRA is restricted by tight junctions alone and that 70 kDa dextran is restricted by both tight junctions and adherens junctions, consistent with the literature. However, other possibilities remain, including altered endocytosis or phagocytosis affecting transcellular permeability after occludin siRNA treatment in the ARPE-19 cells.

A surprising outcome of these studies is that occludin contributes to growth control in ARPE-19 cells. Alterations in growth were examined as a potential route for increased permeability, but blockade of the cell cycle demonstrated that the change in cell division did not cause the increased TAMRA permeability after occludin depletion. Recent studies have implicated tight junction proteins in regulating rates of cell proliferation.[22,29,47] The tight junction protein ZO-1 has been shown to regulate cell division through binding and sequestering the transcription factor ZONAB at the cell border.[47] Additionally, exogenous expression of occludin was sufficient to reverse a raf-transformed phenotype.[29] The present results support these previous findings and demonstrate for the first time an increase in cell division rates with direct occludin content reduction.

FIGURE 6. Paracellular permeability is independent of cell division rates. ARPE-19 cells were treated with control (CN) and occludin-targeted siRNA (siRNA). Graphs display mean and SEM values. (**A**) Tritiated thymidine incorporation was measured in ARPE-19 monolayers ($n = 5$). Treatment with aphidicolin or roscovitine blocked tritiated thymidine incorporation and eliminated any effect of occludin siRNA on DNA synthesis. ARPE-19 monolayers were assessed for (**B**) TER (DMSO, $n = 29$; aphidicolin, $n = 2$; roscovitine, $n = 18$) and permeability to (**C**) 70 kDa dextran ($n = 12$–14) and (**D**, **E**) TAMRA ($n = 19$–22) under diffusive conditions. Inhibition of cell division had no significant effect on TER or solute permeability. Statistical significance was determined by ANOVA (*$P < 0.05$; ***$P < 0.001$).

Thus, this study demonstrated for the first time that RPE cells have an adaptive response like that of endothelial cells and that occludin contributes to the cell's adaptive response after pressure application. Further, occludin has a separate function in controlling cell division. These studies support a role for occludin in the regulation of barrier properties, particularly in response to changes in environmental stressors, and demonstrate a novel role of occludin in the regulation of cell growth.

References

1. Gonzalez-Mariscal L, Betanzos A, Nava P, Jaramillo BE. Tight junction proteins. *Prog Biophys Mol Biol*. 2003;81:1–44.
2. Miyoshi J, Takai Y. Molecular perspective on tight-junction assembly and epithelial polarity. *Adv Drug Deliv Rev*. 2005;57:815–855.
3. Marmor MF, Wolfensberger TJ. *The Retinal Pigment Epithelium: Function and Disease*. New York: Oxford University Press; 1998.
4. Korte GE, Burns MS, Bellhorn RW. Epithelium-capillary interactions in the eye: the retinal pigment epithelium and the choriocapillaris. *Int Rev Cytol*. 1989;114:221–248.
5. Vinores SA, Kuchle M, Derevjanik NL, et al. Blood-retinal barrier breakdown in retinitis pigmentosa: light and electron microscopic immunolocalization. *Histol Histopathol*. 1995;10:913–923.
6. Vinores SA, Derevjanik NL, Ozaki H, Okamoto N, Campochiaro PA. Cellular mechanisms of blood-retinal barrier dysfunction in macular edema. *Doc Ophthalmol*. 1999;97:217–228.
7. Kausalya PJ, Amasheh S, Gunzel D, et al. Disease-associated mutations affect intracellular traffic and paracellular Mg^{2+} transport function of Claudin-16. *J Clin Invest*. 2006;116:878–891.
8. Wolburg H, Wolburg-Buchholz K, Liebner S, Engelhardt B. Claudin-1, claudin-2 and claudin-11 are present in tight junctions of choroid plexus epithelium of the mouse. *Neurosci Lett*. 2001;307:77–80.
9. Wen H, Watry DD, Marcondes MC, Fox HS. Selective decrease in paracellular conductance of tight junctions: role of the first extracellular domain of claudin-5. *Mol Cell Biol*. 2004;24:8408–8417.
10. Nitta T, Hata M, Gotoh S, et al. Size-selective loosening of the blood-brain barrier in claudin-5-deficient mice. *J Cell Biol*. 2003;161:653–660.
11. Van Itallie CM, Fanning AS, Anderson JM. Reversal of charge selectivity in cation or anion-selective epithelial lines by expression of different claudins. *Am J Physiol Renal Physiol*. 2003;285:F1078–F1084.
12. Turksen K, Troy TC. Barriers built on claudins. *J Cell Sci*. 2004;117:2435–2447.
13. Hirase T, Staddon JM, Saitou M, et al. Occludin as a possible determinant of tight junction permeability in endothelial cells. *J Cell Sci*. 1997;110(pt 14):1603–1613.
14. Antonetti DA, Barber AJ, Khin S, Lieth E, Tarbell JM, Gardner TW. Vascular permeability in experimental diabetes is associated with reduced endothelial occludin content: vascular endothelial growth factor decreases occludin in retinal endothelial cells: Penn State Retina Research Group. *Diabetes*. 1998;47:1953–1959.
15. The effect of intensive treatment of diabetes on the development and progression of long-term complications in insulin-dependent diabetes mellitus: the Diabetes Control and Complications Trial Research Group. *N Engl J Med*. 1993;329:977–986.
16. Mitic LL, Anderson JM. Molecular architecture of tight junctions. *Annu Rev Physiol*. 1998;60:121–142.
17. Burgel N, Bojarski C, Mankertz J, Zeitz M, Fromm M, Schulzke JD. Mechanisms of diarrhea in collagenous colitis. *Gastroenterology*. 2002;123:433–443.
18. Jin M, Barron E, He S, Ryan SJ, Hinton DR. Regulation of RPE intercellular junction integrity and function by hepatocyte growth factor. *Invest Ophthalmol Vis Sci*. 2002;43:2782–2790.
19. Abe T, Sugano E, Saigo Y, Tamai M. Interleukin-1β and barrier function of retinal pigment epithelial cells (ARPE-19): aberrant expression of junctional complex molecules. *Invest Ophthalmol Vis Sci*. 2003;44:4097–4104.
20. Giebel SJ, Menicucci G, McGuire PG, Das A. Matrix metalloproteinases in early diabetic retinopathy and their role in alteration of the blood-retinal barrier. *Lab Invest*. 2005;85:597–607.
21. Nusrat A, Brown GT, Tom J, et al. Multiple protein interactions involving proposed extracellular loop domains of the tight junction protein occludin. *Mol Biol Cell*. 2005;16:1725–1734.
22. Vietor I, Bader T, Paiha K, Huber LA. Perturbation of the tight junction permeability barrier by occludin loop peptides activates beta-catenin/TCF/LEF-mediated transcription. *EMBO Rep*. 2001;2:306–312.
23. Wong V, Gumbiner BM. A synthetic peptide corresponding to the extracellular domain of occludin perturbs the tight junction permeability barrier. *J Cell Biol*. 1997;136:399–409.

24. Tavelin S, Hashimoto K, Malkinson J, Lazorova L, Toth I, Artursson P. A new principle for tight junction modulation based on occludin peptides. *Mol Pharmacol*. 2003;64:1530–1540.

25. Lacaz-Vieira F, Jaeger MM, Farshori P, Kachar B. Small synthetic peptides homologous to segments of the first external loop of occludin impair tight junction resealing. *J Membr Biol*. 1999;168:289–297.

26. Yu AS, McCarthy KM, Francis SA, et al. Knockdown of occludin expression leads to diverse phenotypic alterations in epithelial cells. *Am J Physiol Cell Physiol*. 2005;288:C1231–C1241.

27. Saitou M, Furuse M, Sasaki H, et al. Complex phenotype of mice lacking occludin, a component of tight junction strands. *Mol Biol Cell*. 2000;11:4131–4142.

28. Schulzke JD, Gitter AH, Mankertz J, et al. Epithelial transport and barrier function in occludin-deficient mice. *Biochim Biophys Acta*. 2005;1669:34–42.

29. Wang Z, Mandell KJ, Parkos CA, Mrsny RJ, Nusrat A. The second loop of occludin is required for suppression of Raf1-induced tumor growth. *Oncogene*. 2005;24:4412–4420.

30. Salathe EP, Venkataraman R. Interaction of fluid movement and particle diffusion across capillary walls. *J Biomech Eng*. 1982;104:57–62.

31. Baetscher M, Brune K. An in vitro system for measuring endothelial permeability under hydrostatic pressure. *Exp Cell Res*. 1983;148:541–547.

32. Turner MR. Flows of liquid and electrical current through monolayers of cultured bovine arterial endothelium. *J Physiol*. 1992;449:1–20.

33. DeMaio L, Tarbell JM, Scaduto RC Jr, Gardner TW, Antonetti DA. A transmural pressure gradient induces mechanical and biological adaptive responses in endothelial cells. *Am J Physiol*. 2004;286:H731–H741.

34. Suttorp N, Hessz T, Seeger W, et al. Bacterial exotoxins and endothelial permeability for water and albumin in vitro. *Am J Physiol*. 1988;255:C368–C376.

35. Harhaj NS, Barber AJ, Antonetti DA. Platelet-derived growth factor mediates tight junction redistribution and increases permeability in MDCK cells. *J Cell Physiol*. 2002;193:349–364.

36. Livak KJ, Schmittgen TD. Analysis of relative gene expression data using real-time quantitative PCR and the $2(-\Delta\Delta C(T))$ method. *Methods*. 2001;25:402–408.

37. DeMaio L, Antonetti DA, Scaduto RC Jr, Gardner TW, Tarbell JM. VEGF increases paracellular transport without altering the solvent-drag reflection coefficient. *Microvasc Res*. 2004;68:295–302.

38. Chihara E, Nao-i N. Resorption of subretinal fluid by transepithelial flow of the retinal pigment epithelium. *Graefe's Arch Clin Exp Ophthalmol*. 1985;223:202–204.

39. Miller SS, Hughes BA, Machen TE. Fluid transport across retinal pigment epithelium is inhibited by cyclic AMP. *Proc Natl Acad Sci U S A*. 1982;79:2111–2115.

40. Balda MS, Whitney JA, Flores C, Gonzalez S, Cereijido M, Matter K. Functional dissociation of paracellular permeability and transepithelial electrical resistance and disruption of the apical-basolateral intramembrane diffusion barrier by expression of a mutant tight junction membrane protein. *J Cell Biol*. 1996;134:1031–1049.

41. McCarthy KM, Skare IB, Stankewich MC, et al. Occludin is a functional component of the tight junction. *J Cell Sci*. 1996;109(pt 9):2287–2298.

42. Barrios-Rodiles M, Brown KR, Ozdamar B, et al. High-throughput mapping of a dynamic signaling network in mammalian cells. *Science*. 2005;307:1621–1625.

43. Hou J, Gomes AS, Paul DL, Goodenough DA. Study of claudin function by RNA interference. *J Biol Chem*. 2006;281:36117–36123.

44. Tinsley JH, Breslin JW, Teasdale NR, Yuan SY. PKC-dependent, burn-induced adherens junction reorganization and barrier dysfunction in pulmonary microvascular endothelial cells. *Am J Physiol Lung Cell Mol Physiol*. 2005;289:L217–L223.

45. Liebner S, Cavallaro U, Dejana E. The multiple languages of endothelial cell-to-cell communication. *Arterioscler Thromb Vasc Biol*. 2006;26:1431–1438.

46. Muller SL, Portwich M, Schmidt A, et al. The tight junction protein occludin and the adherens junction protein alpha-catenin share a common interaction mechanism with ZO-1. *J Biol Chem*. 2005;280:3747–3756.

47. Balda MS, Matter K. The tight junction protein ZO-1 and an interacting transcription factor regulate ErbB-2 expression. *EMBO J*. 2000;19:2024–2033.